Numerical and experimental study of the distribution of charged species in a flat stoichiometric premixed $CH_4/O_2/Ar$ flame

Jie Han, Awad B.S. Alquaity, Memdouh Belhi*, Aamir Farooq, S. Mani Sarathy, Fabrizio Bisetti
Clean Combustion Research Center, King Abdullah University of Science and Technology(KAUST), Saudi Arabia

Abstract

In this paper, an existing ion reaction mechanism is used to compute the distribution of charged species in a flat stoichiometric premixed $CH_4/O_2/Ar$ flame stabilized on top of a McKenna burner. The ion reaction rates and charged species thermodynamic data are updated according to the most recent data. A modified version of the detailed ARAMCO 1.3 reaction mechanism is used to describe the chemistry of neutral species. Because of the important role of CH in the chemi-ionization process, its prediction is improved based on the available measured data. The ability of the ion reaction mechanism to predict the distribution of positive ions is assessed by comparing to the experimental measurements performed in our group. The calculated results are qualitatively consistent with the experimental data, even though there exist quantitative differences that need to be addressed in future work.

Introduction

In flames, charged species are generated naturally by a chemi-ionization process [1]. They may play an important role when an electric field is applied to a flame. Improving flame stabilization [2] and reducing pollutant emissions [3] are among the observed effects of the charged species interaction with electric fields.

Numerical modeling of the electric field interaction with combustion requires chemistry models capable of calculating the distribution of charged species in flames. Approaches to treat the ion chemistry in flames are scarce in the literature and definitive reaction mechanisms are unavailable. The authors of Refs. [4, 5] describe a mechanism for the formation of ions in premixed acetylene flames. This mechanism includes 62 ion reactions involving 12 positive ions and excluding negative ions. Pedersen et al. [6] study the distribution of ions in methane flames. Their mechanism includes 13 ion reactions, 5 positive ions and still excludes anions. Hu et al. [7] and Yamashita et al. [8], who investigated the interaction between the electric field and combustion, employed mechanisms with less ion reactions, respectively 3 and 11. Negative ions are also neglected.

More recently, Prager et al. [9, 10] proposed a reaction mechanism accounting for 67 ions reactions including 4 cations, 6 anions and electrons. This model represents the most complete inventory of charged species reactions in methane/oxygen flames. It has been successfully used to predict the positive ion densities in lean methane/oxygen flames. The objective of this paper is to assess the ability of that mechanism to predict the distribution of positive ions in stoichiometric flames. Recent experimental measurements, carried out in our group, are used for the evaluation of the chemistry model.

The ion reaction rates and charged species thermodynamic data are updated according to the recent data from the UMIST [11] and Burcat [12] databases, respectively. A modified version of the detailed ARAMCO 1.3 mechanism [13] is employed to describe the chemistry of neutral species. The ARAMCO 1.3 mechanism is modified in order to improve the prediction of CH, which plays an important role in the production process of ions in flames. The improvement of CH prediction relied on the measured data in Ref. [14].

The studied configuration is an atmospheric premixed flat stoichiometric $CH_4/O_2/Ar$ flame. The flame is simulated using the program PREMIX [15]. The aerothermochemistry equations along with a Poisson equation for the electric potential are solved. The electric field is computed from the first derivation of the electric potential. The binary transport coefficients of ions are calculated using the (n,6,4) [16] and Coulomb [17] interaction potentials. A constant value recommended in Ref. [18] is used to describe the mobility of electrons, while their diffusivity is approximated by Einstein's relation.

The paper is organized as follows. First, the experimental and numerical setups are presented. Thereafter, the numerical procedure and chemistry model are described. The developments implemented in the PREMIX code to allow for the simulation of ions and electrons are highlighted. Also, the main modifications introduced in the ARAMCO 1.3 mechanism to improve its CH prediction are presented. Finally, a qualitative comparison of the numerical results to experimental measurements is shown. The distribution of charged species in the flame is analyzed and aspects needing improvement are highlighted.

*Corresponding author: memdouh.belhi@kaust.edu.sa

Experimental configuration

A commercially available water-cooled 6 cm diameter McKenna burner (Holthuis & Associates) is used to produce a premixed stoichiometry methane-oxygen flat flame. The flame is surrounded by an argon shield to avoid reactions with atmospheric air. The flow rate is 8 slpm (standard liters per minute). The temperature of the cooling water entering the burner is kept constant at 15 °C. The flame is at atmospheric pressure. Depending on the need, flames of various equivalence ratio are considered, namely $\Phi = \{0.5, 1, 1.5\}$.

Molecular beam mass spectrometry (MBMS) is a powerful tool to analyze reactive systems. It has been extensively employed to study complex environments such as flames and plasmas. High sensitivity and ability to differentiate ions from neutrals make this technique attractive for studying ion chemistry in flames.

The MBMS system is a modified Hiden HPR 60 system equipped with a triple filter quadrupole mass spectrometer with range 1 to 300 m/z. The experimental setup is shown in Fig. 1. More details on the experimental setup and methods can be found in Ref. [19].

To minimize flow disturbances and interference from the surrounding laboratory air, the flame is confined in a chamber. The McKenna burner is mounted on a vertical translation stage with a minimum step size of 10 μm. A 5 mm long alumina cone with an aperture of 0.1 mm is used for sampling the flame gases. The flame gases are sampled along the centerline of the flame and transferred via a molecular beam to the mass spectrometer using three stages of differential pumping.

The first and second stage skimmer cones have orifice sizes of 0.6 mm and 2 mm, respectively. To facilitate the extraction and transmission of ions along the molecular beam, electrical potentials of -40 V and -20 V are applied to the first stage and second stage skimmer cones, respectively. In the third stage, the ions are transmitted to the quadruple detector using ion optics. The voltage settings on the MBMS were optimized using the MBMS program to obtain maximum detector signal for the flame ions.

The flame temperature is measured using a SiO_2 coated platinum-30% rhodium/platinum 6% rhodium (Type-B, Omega) thermocouple with a bead size of 0.36 mm. Thermocouple readings are corrected for radiation effects [20]. The radiation corrections for thermocouple readings ranged from 40 K to 245 K for flame temperatures between 1085 and 1920 K, respectively.

The MBMS measurements do not provide absolute values of ion number densities. Therefore, the simulation results can only be evaluated qualitatively. The measurements are performed only for positive ions because negative ions are present in trace quantities and are below the sensitivity limit of our MBMS system.

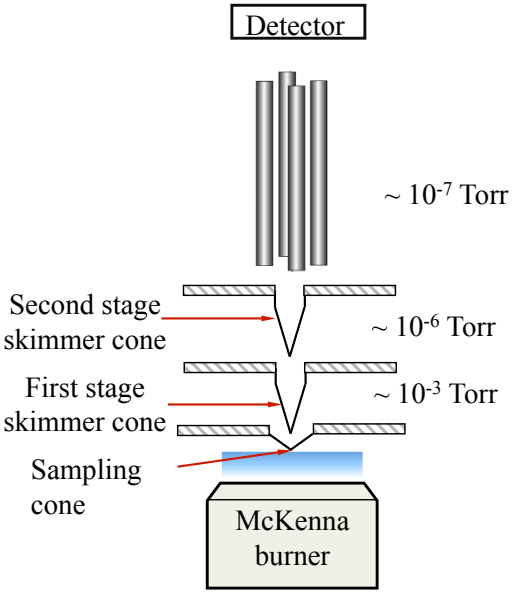

Figure 1: Experimental setup

Numerical procedure and chemical mechanism

The code PREMIX (CHEMKIN II) [15] is used to simulate the flame described above. The experimental flame is modeled as a 1D burner stabilized premixed flat flame. To determine the internal electric field of the flame, the Poisson equation for the electric potential is solved by the boundary value problem solver TWOPNT:

$$\frac{d^2V}{dx^2} = -\frac{e}{\epsilon_0}\sum_i q_i n_i, \tag{1}$$

where V is the electric potential, $e = 1.6 \times 10^{19}$ C is the elementary charge, $\epsilon_0 = 8.85 \times 10^{12}$ F/m is the vacuum permittivity, n_i and q_i are the number density and the charge number of the species i, respectively. The electric potential is set to zero at both cold and hot boundaries. The electric field strength E is determined from the electric potential as:

$$E = -\frac{dV}{dx}, \tag{2}$$

and the mass flux for charged species J_i is modified to include the drift diffusion flux:

$$\mathbf{J}_i = -D_i\nabla(n_i) + \frac{q_i}{|q_i|}\mu_i\mathbf{E}n_i, \tag{3}$$

D_i and μ_i are the mixture-averaged diffusivity and mobility of the charged species i, respectively. The transport coefficients of ions are calculated from Blanc's law [16, 21] and ion binary transport coefficients. The ion-neutral and ion-charge interactions are described by using the (n,6,4) [16] and Coulomb [17] interaction potentials, respectively. A constant

value of 0.4 $m^2 \cdot V^{-1} \cdot s^{-1}$, recommended in Ref. [18], is used to describe the electron mobility. The Einstein relation is used to calculate the electron diffusivity:

$$\mu_i = D_i \frac{q_i}{k_B T}, \quad (4)$$

where k_B is the Boltzmann constant and T is temperature. As the heat loss, produced in the experiment, cannot be quantified numerically, the energy equation is not solved and the experimental profile of temperature is used in the simulations.

Based on the experimental works of Goodings et al. [22, 23], Prager et al. [9, 10] developed a detailed ion reaction mechanism to describe the chemistry of charged species in lean-to-stoichiometric methane/oxygen flames. But they applied their kinetic mechanism only to a lean flame. The chemistry of charged species is presented by 67 reversible reactions including 11 charged species.

The chemistry model of charged species includes 4 cations (H_3O^+, $C_2H_3O^+$, CH_5O^+, and HCO^+), 6 anions (O_2^-, O^-, OH^-, CHO_2^-, CHO_3^-, and CO_3^-) and electrons. The main channels responsible for ion chemistry in flames are illustrated schematically in Fig. 2.

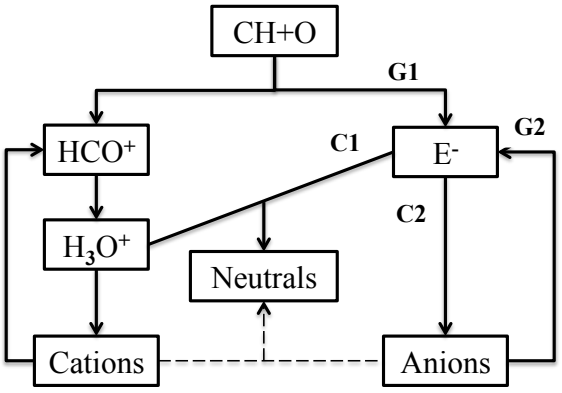

Figure 2: Flowchart of ion chemistry. G1 and G2 are the channels generating E^-. C1 and C2 are the channels consuming E^-.

Positive ions and electrons are produced as a result of the interaction of the radicals CH and O. This reaction is known as the chemi-ionization process and it is generally considered as the source of ions in lean and stoichiometric flames. The first cation HCO^+ undergoes a proton transfer reaction and it is rapidly transformed into the hydronium ion H_3O^+. In the burnt gases, electrons recombine with H_3O^+ to produce neutrals. This recombination, presented by C1 in the flowchart, is responsible for the slow decrease of the number density of H_3O^+ in the burnt gases. As a result of ion/molecule reactions, H_3O^+ also forms other cations. Electrons attach to selected neutral species, such as O_2, O, and OH, to generate primary anions. These reactions are presented by C2 in the flowchart. The produced negative ions also form other anions via ion/molecule reactions or participate in associative electron detachment reactions. The last process presents an important source of anion loss in the region of burnt gases. Some anions and cations recombine to form neutrals, but this recombination process can be neglected because of the low concentrations of participating positive ions.

The ion reaction model described above is employed to calculate the distribution of ions in the stoichiometric flame investigated in this study. The ion reaction rates and charged species thermodynamic data are updated according to the recent data from the UMIST [11] and Burcat [12] databases, respectively. If the rate constant of a reaction is unavailable in the UMIST database, the ADO (averaged dipole orientation) theory [24] is used to calculate its value. The required data on polarizability and dipole moment of reactants are taken from the Computational Chemistry Comparison and Benchmark DataBase [25].

As can be observed from the ion reaction flowchart (Fig. 2), the neutral species CH plays an essential role in the formation of ions in the flame. Therefore, its accurate prediction is necessary to simulate the distribution of charged species adequately. The GRI 3.0 neutral mechanism, which contains 325 reactions and 53 species, has the ability to predict well the distribution of CH [26]. However, it is not suitable for hydrocarbon fuels having more than two atoms of carbon. In contrast, the ARAMCO 1.3 reaction mechanism, which includes 1542 reactions and 253 species, is effective in handling the kinetics of both lighter and heavier fuels [13].

Figure 3 compares the CH predictions from ARAMCO 1.3 and GRI 3.0 mechanisms to the experimental measurements [14]. The results are obtained from a 1D premixed flame burning a stoichiometric $CH_4/O_2/N_2$ mixture at a pressure of 25 torr. The profile of the CH mole fraction obtained using the GRI 3.0 mechanism compares well to the experiment. However, the CH predictions from the ARAMCO 1.3 mechanism [13] are not satisfactory.

By comparing the reaction pathway of CH in GRI 3.0 and ARAMCO 1.3, it is found that both mechanisms result in the same pathways to the formation of CH: $CH_4 \longrightarrow CH_3 \longrightarrow CH_2(S) \longrightarrow CH_2 \longrightarrow CH$. Two modifications are thus implemented in the ARAMCO 1.3 mechanism [13]. First, the rate of the reaction $CH_3 + OH \rightleftharpoons CH_2(S) + H_2O$ are increased at low pressure (p=0.01 and 0.1 atm) by 5 times [27, 28]. This reaction is a pressure dependent reaction and it is written in the PLOG form. Second, the rate of the reaction $CH_2 + H \rightleftharpoons CH + H_2$ suggested in [29] is used. Moreover, the rate of the reaction $CH + O_2 \rightleftharpoons CO + OH^*$ is changed as suggested in [30]. This reaction presents the main channel to

form OH^*. As a result of those three modifications, the prediction of CH and OH^* using ARAMCO 1.3 mechanism is significantly improved, but it is still less accurate than that obtained by the GRI 3.0 mechanism (see Fig. 3).

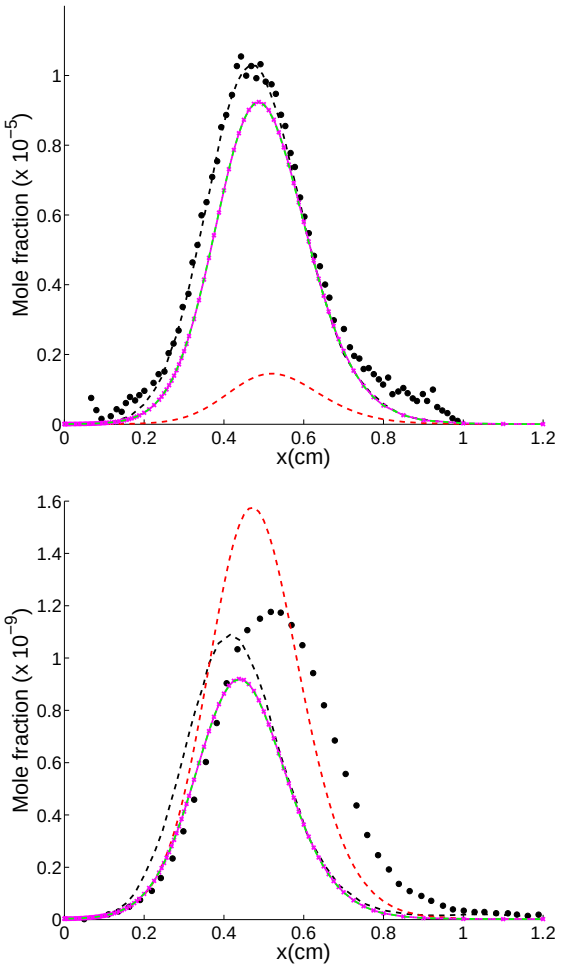

Figure 3: Mole fractions of CH (top) and OH^* (bottom) in comparison with the experimental measurements. Experimental data is shown as black symbols and are taken from Ref. [14] for CH and Ref. [31] for OH^*. Black and red dashed lines represent the simulation results from GRI 3.0 [14] and Aramco 1.3 [13] mechanisms, respectively. The mole fractions of OH^* obtained using ARAMCO 1.3 are divided by a factor of 20. Pink and green lines refer to the mole fractions from the modified ARAMCO 1.3 and its reduced version (removing species having more than two carbon atoms), respectively.

The ARAMCO 1.3 mechanism is used in the simulations in order to support the development of ion chemistry for heavier fuels in the future. In this study, reactions including species having more than two atoms of carbon are removed from the mechanism, because they increase significantly the computational cost without having any important role in CH_4 flames. The mechanism used in all simulations contains 487 reactions and 88 neutral species.

Results

As the quantification of the amount of heat losses is over the scope of this paper, the experimental profile is used in the simulation instead of solving the energy equation. Recall that the objective of this paper is the assess the ability of the ion reaction mechanism to reproduce the experimental distribution of ions. The experimental profile of temperature is measured with thermocouples as discussed in the methods section. The profile is shown in Fig. 4 .

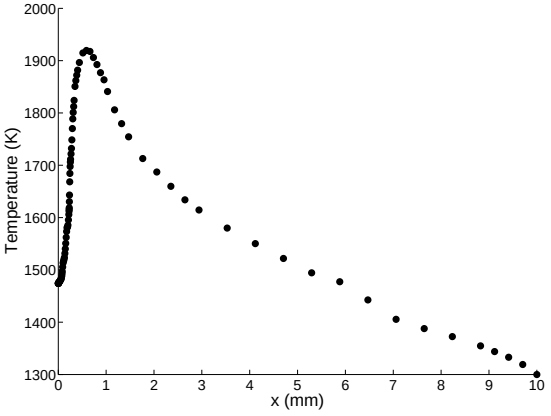

Figure 4: The experimental profile of temperature used in the calculation.

The size of the calculation domain is extended upstream the burner face by 1 cm so that the cold boundary gradients vanish. This allows for improving the qualitative comparison with experiment, even though that effect is unclear. The temperature profile is extrapolated to room temperature in the extended zone.

In Figure 5, the simulation results for the number densities of cations are compared to the experimental measurements. Because integrated signals [19] are measured instead of ions densities, the experimental data is scaled so that the maximum experimental and numerical number densities of the most abundant ion, which is H_3O^+, are matched. We are assuming that the integrated signals generated by the ions are proportional to their number densities. The shape of the profiles as well as the ratio between the peak number densities of the cations are well reproduced. The difference between the axial location of the peak number densities of individual ions is also consistent with experiment. However, the agreement of the location of simulated peak ion densities with those from the experiment is less satisfactory. The ion densities increase earlier in the cold gas region compared to experiments. The source of those differences are being

investigated. It may be that, due to the flame stabilizing very close to the burner surface, the role of the burner may not be ignored in the numerical model.

From Fig. 5, it is clear that the ion $C_2H_3O^+$ dominates the region upstream the reaction zone, but H_3O^+ is generally the most abundant ion in the flame. The peaks of the number densities of CH_5O^+ and $C_2H_3O^+$ are obtained upstream but close to the reaction zone, while that of H_3O^+ is located in the region where heat release is maximum. The profile of HCO^+ is not presented because it has very small number densities and can be neglected.

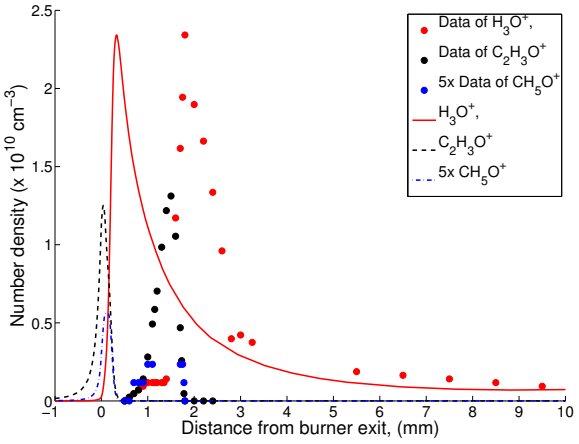

Figure 5: Distribution of positive ions across the flame in comparison with experiment.

In Figure 6, the individual negative charged species profiles are presented. Because of the lack of experimental data on the distribution of negative charged species, the ability of the ion reaction mechanism to predict the distribution of anions and electrons cannot be assessed.

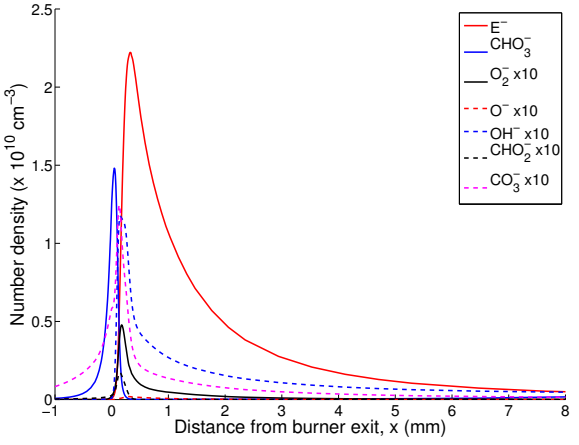

Figure 6: Distribution of negative charged species across the flame.

With the exception of CHO_3^-, the other five anions have very low concentrations. The concentrations of CHO_3^- are of the same order of magnitude as the abundant positive ions. The CHO_3^- peak is located upstream the reaction zone at practically the same position as $C_2H_3O^+$ peak, but it vanishes in the burnt gas region. The other negative ions occur downstream of the reaction zone. The total negative charge in the flame is dominated by electrons having densities comparable to those of H_3O^+.

The simulation results of the total number densities of positives ions, negative ions and electrons are shown in Fig. 7. The positive ion concentration in close-to-stoichiometry flames of hydrocarbons usually ranges from 10^{10} up to 10^{11} cm^{-3} [32]. Present simulations are in good agreement with this order of magnitude. The maximum positive ion number density corresponds to 2.45×10^{10} cm^{-3} and that of electrons to 2.25×10^{10} cm^{-3}. They are located in the region where the temperature is maximum. This is expected, since the rate of chemi-ionization peaks in this zone. The cations undergo recombination reactions with electrons leading to the formation of neutrals. This justifies the gradual decrease in their number densities in the region of burnt gases.

The peak of the total ion negative density (1.58×10^{10} cm^{-3}) is obtained is the region of low temperature located upstream the reaction zone. In this region, the attachment of electrons with oxygen molecules through three-body reactions is a major process. This may therefore justify the high number density of negative ions in this zone. The negative ions interact with neutral species through associative electron detachment reactions. This process represents a considerable loss of anions in the flame, and then may explain the low anion densities in the region downstream the reaction zone.

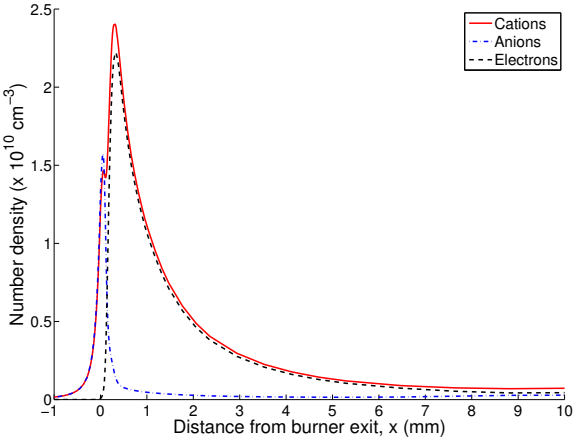

Figure 7: Distribution of the total number densities of cations, anions and electrons across de flame.

Conclusions

A chemistry model to compute the distribution of ions in flames is applied to a stoichiometric flat $CH_4/O_2/Ar$ flame. Rate constants of charged species

reactions are updated according to the most recent data. The combustion of neutral species is represented by the detailed ARAMCO 1.3 mechanism, which is modified in order to improve the prediction of CH. This improvement is motivated by the fact that CH plays important role in the process of chemi-ionization.

The approach used for the chemistry is evaluated by comparing to recent experimental measurements performed in our group. Overall, the simulations recover qualitatively the experimental distribution of positive ions. Because of the lack of absolute values of ion densities, the performance of the ion reaction mechanism to predict the densities of ions quantitatively cannot be assessed at this time. More experimental measurements on the number densities of both positive and negative charged species in lean-to-rich flames are ongoing.

References

[1] H.F. Calcote. In *Eighth Symposium (International) on Combustion*, volume 8, pages 184–199, 1961.

[2] S.M Lee, C.S. Park, M.S. Cha, and S.H. Chung. *IEEE Transactions on Plasma Science*, 33(5):1703–1709, 2005.

[3] M. Saito, T. Arai, and M. Arai. *Combust. Flame*, 119(3):356–366, 1999.

[4] R.C. Brown and A.N. Eraslan. *Combust. Flame*, 73(1):1–21, 1988.

[5] A.N. Eraslan and R.C. Brown. *Combust. Flame*, 74(1):19–37, 1988.

[6] T. Pedersen and R.C. Brown. *Combust. Flame*, 94(4):433–448, 1993.

[7] J. Hu, B. Rivin, and E. Sher. *Exp. Therm. Fluid Sci.*, 21(1):124–133, 2000.

[8] K. Yamashita, S. Karnani, and D. Dunn-Rankin. *Combust. Flame*, 156(6):1227–1233, 2009.

[9] J. Prager. *Modeling and Simulation of Charged Species in Lean Methane-Oxygen Flames*. Thesis, 2005.

[10] J. Prager, U. Riedel, and J. Warnatz. In *Proc. Combust. Inst.*, volume 31, pages 1129–1137, 2007.

[11] The umist database for astrochemistry http://www.udfa.net/, 2012.

[12] A. Burcat. Ideal gas thermodynamic data in polynomial form for combustion and air pollution use, http://garfield.chem.elte.hu/burcat/burcat.html, 2006.

[13] Wayne K. Metcalfe, Sinad M. Burke, Syed S. Ahmed, and Henry J. Curran. *Int. J. Chem. Kinet.*, 45(10):638–675, 2013.

[14] P.A. Berg, D.A. Hill, A.R. Noble, G.P. Smith, J.B. Jeffries, and D.R. Crosley. *Combust. Flame*, 121(1-2):223–235, 2000.

[15] R. J. Kee, J. F. Grcar, M. D. Smooke, and J. A. Miller. A fortran program for modeling steady laminar one-dimensional premixed flames. *Sandia National Laboratories Report*, SAND85-8240, 1985.

[16] E.A.Mason and E.W.McDaniel. *Transport Properties of Ions in Gases*. John Wiley & Sons, Inc., 1988.

[17] E.A. Mason, R.J. Munn, and J.F. Smith. *Phys. Fluids*, 10(8):DOI: 10.1063/1.1762365, 1967.

[18] F. Bisetti and M.E. Morsli. *Combust. Flame*, 159(12):3518–3521, 2012.

[19] A.B.S Alquaity, N. Hourani, H.S.M. Chahine, S.M. Sarathy, and A Farooq. In *50th AIAA/ASME/SAE/ASEE Joint Propulsion Conference, Cleveland, OH*, July 28-30, 2014.

[20] V. Hindasageri, R.P. Vedula, and S.V. Prabhu. *Rev. Sci. Instrum.*, 84:024902, 2013.

[21] R.V. Chiflikian. *Phys. Plasmas*, 2(10):3902–3909, 1995.

[22] J.M. Goodings, D.K. Bohme, and C.W. Ng. *Combust. Flame*, 36:27–43, 1979.

[23] J.M. Goodings, D.K. Bohme, and C.W. Ng. *Combust. Flame*, 36:45–62, 1979.

[24] S. Timothy, Elkie S.C.F., and M.T. Bowers. *J. Chem. Phys.*, 69(5):2243–2250, 1978.

[25] D. Johnson III Russell. Nist computational chemistry comparison and benchmark database, http://cccbdb.nist.gov/, 16a, August, 2013.

[26] G.P. Smith, D.M. Golden, M. Frenklach, N.W. Moriarty, B. Eiteneer, M. Goldenberg, C.T. Bowman, R.K. Hanson, S. Song, W.C.J. Gardiner, V.V. Lissianski, and Z. Qin. http://www.me.berkeley.edu/grimech/, 2000.

[27] S. Mani Sarathy and A.W. Jasper. *Private communication*, 2014.

[28] S. Mani Sarathy, J. Han, H. Curran, and C. Zhou. *Private communication*, 2014.

[29] D. L. Baulch, C. T. Bowman, C. J. Cobos, R. A. Cox, Th. Just, J. A. Kerr, M. J. Pilling, D. Stocker, J. Troe, W. Tsang, R. W. Walker, and J. Warnatz. *J. Phys. Chem.*, Ref. Data 34:757, 2005.

[30] Trupti Kathrotia. *Reaction Kinetics Modeling of OH*, CH* and C2* Chemiluminescence*. Thesis, 2011.

[31] P.G. Smith, J. Luquea, C. Parka, J.B. Jeffriesa, and D.R. Crosleya. *Combust. Flame*, 131(1-2):59–69, 2002.

[32] A.B. Fialkov. *Prog. Energy Combust. Sci.*, 23(5-6):399–528, 1997.